Journal of The Electrochemical Society, **153** (9) A1714-A1718 (2006)
0013-4651/2006/153(9)/A1714/5/$20.00 © The Electrochemical Society

Electro-oxidation of Methanol on Pt Particles Dispersed on RuO_2 Nanorods

Yan-Juan Gu and Wing-Tak Wong[z]

Department of Chemistry, University of Hong Kong, Hong Kong, China

The successful attachment of 1–3 nm Pt nanoparticles to the surface of amine-functional RuO_2 nanorods through a simple, two-step chemically controlled procedure is reported here. The nanocomposites were characterized by transmission electron microscopy (TEM) and X-ray diffraction. TEM images showed that the monodispersed Pt nanoparticles were highly stable against thermal treatment. The electro-oxidation of methanol in sulfuric acidic solution was studied on RuO_2-supported Pt nanoparticles by cyclic voltammetry and chronoamperometry. All of the electrochemical results show that RuO_2/Pt catalysts exhibit high activity for methanol oxidation that results from the high electroactive surface area of Pt nanoparticles and the effect of RuO_2. These results demonstrate the feasibility of using metal oxide nanorods in certain fuel cell applications.
 [DOI: 10.1149/1.2217327]

Manuscript submitted January 23, 2006; revised manuscript received May 1, 2006. Available electronically July 14, 2006.

Platinum is the most widespread and promising electrocatalyst for the oxidation of small organic molecules such as methanol. However, the performance of pure Pt electrodes is often hindered due to the formation of strongly adsorbed intermediates, such as carbon monoxide, which poison the electrode surface during the adsorption and electro-oxidation of methanol. Significant efforts are being dedicated to the design and synthesis of a Pt-based alloy catalyst with a higher poison tolerance and greater methanol oxidation activity. Various binary systems, such as the Pt-Ru,[1-5] Pt-W,[6-8] Pt-Mo,[7] Pt-Sn,[9,10] Pt-Ni,[11,12], and Pt-Os[13,14] catalyst systems have been investigated recently, and have shown improved activity for hydrogen oxidation reaction in the presence of CO. To date, the incorporation of Ru into the Pt catalyst has yielded the best results. However, the precise reason for the superior performance of the binary catalyst is unclear. It is currently accepted that to minimize the effect of the poisonous species, the cocatalyst must have a larger tendency to form oxides than Pt. This induces the electrosorption of oxygen-containing species O[H] at a lower potential, which can take part in the CO oxidation reaction that removes it from the surface through the so-called bifunctional mechanism.[15-17] Based on this mechanism, metal oxides have been introduced to form cocatalysts to enhance activity toward methanol electro-oxidation.[18-20] All of these cocatalysts have shown improved performance for methanol oxidation in comparison to the platinized glassy carbon (GC) electrode. Ruthenium dioxide (RuO_2) is an important electrode material for applications in electrocatalysis and power sources as it exhibits excellent corrosion resistance in acidic media, good electrical conductivity, and high electrocatalytic activity toward oxygen evolution.[21,22] Recent studies have demonstrated the importance of hydrous RuO_2 in the Pt-Ru direct methanol fuel cell catalyst.[23,24] However, contrary reports have suggested that the formation of ruthenium oxides may cause the deactivation of the Pt-Ru electrocatalyst,[25] and surface RuO_x species have been observed on the Pt-Ru/C anode. Several recent reports have discussed the synthesis of RuO_2/Pt nanocomposites by the sol-gel method,[26-29] in which a mixture of anhydrous RuO_2 or $RuO_2 \cdot XH_2O$ nanoparticles supported Pt nanoparticles. They also demonstrated an enhancing effect of RuO_2/Pt nanocomposites on the oxidation of methanol. However, very little work has focused on the use of the single-crystal structure of RuO_2 nanorods as supporting material. These nanorods mainly exhibit the (110) plane nanorod sidewall. It has been shown that RuO_2-based catalysts are much more active in the oxidation of CO than related metallic Ru catalysts because of the weak oxygen surface bonding of bridging O atoms on RuO_2(110) in comparison to the strongly chemisorbed oxygen on Ru(0001).[30,31]

Herein, we report a facile, highly reproducible two-step synthetic process that enables the attachment of 1–3 nm Pt nanoparticles to the (3-aminopropyl)triethoxysilane (APTES)-coated single-crystal structure of RuO_2 nanorods with lengths of around 100 nm. This work exploits the strong ability of carboxylic acid-terminated Pt nanoparticles to bind to the terminal $-NH_2$ groups of organic entities, which can be enhanced by mutually attractive electrostatic interactions when the two components are oppositely charged. We also investigate the effect of RuO_2 nanorods on the electrocatalytic properties of Pt nanoparticles using the electro-oxidation of methanol as a probe. The electrocatalytic activity toward the oxidation of methanol is studied by potential sweeps for RuO_2/Pt electrodes of different Pt loading compositions.

Experimental

Synthesis of RuO_2/Pt nanocomposites.— A general synthesis process of RuO_2 nanorods has been described.[32] For the synthesis of the RuO_2/Pt nanocomposite material, the first step is to functionalize the RuO_2 nanorods with APTES.[33,34] The hydroxyl groups on the oxide surface react with the ethoxy group of the APTES molecules with the formation of Si–O bonds and leave the terminal $-NH_2$ groups available for nanoparticle attachment. In a typical procedure, 30 mg RuO_2 was dispersed with 25 mL absolute ethanol and 25 mL distilled water, and sonicated for 15 min. The resulting solution was transferred to a three-neck flask that was equipped with a condenser and thermometer. Then, 0.5 mL of APTES was injected into the flask and the mixture was vigorously stirred at room temperature for about 1 h before heating to reflux for 2 h under protection with argon at 80°C. After the mixture was cooled to room temperature, the solid product was filtered, washed with ethanol, and then redispersed in 50 mL of ethanol by sonicating for 15 min. To induce positive charges at the surface of the APTES-coated RuO_2, 10 drops of 2 M HNO_3 solution were introduced into the ethanolic dispersion of APTES-coated RuO_2 nanorods, and stirred for 2 h. The second step in the synthesis of the RuO_2/Pt nanocomposite is the attachment of Pt nanoparticles onto APTES-coated RuO_2 nanorods. Highly crystalline Pt nanoparticles were prepared using ethylene glycol as a reducing and stabilizing agent.[35,36] In a typical experiment, 1.5 mL 0.05 M H_2PtCl_6 was added in 50 mL of ethylene glycol that contained 0.1 M NaOH. The solutions were stirred for 30 min in air at room temperature, subsequently heated under reflux to 160°C for 3 h, and then cooled in air. Dark-brown solutions that contained the Pt colloids were formed. Once prepared, the negatively charged Pt nanoparticles that were contained in the colloidal solution were attached to the surface of amino silane-coated RuO_2 nanorods. Thus, the colloidal Pt solution was introduced into a round-bottom flask that contained 50 mL of the ethanolic dispersion of amine-functionalized RuO_2 nanorods, and the mixture was stirred overnight at room temperature. The solid product was filtered, washed with ethanol and distilled water to remove the excess of Pt particles, and then heated at 400°C overnight to remove the organic stabilizers on the Pt nanoparticle surface. The different amounts of

[z] E-mail: wtwong@hkucc.hku.hk

Pt metal loading were prepared by controlling the additional volume of Pt nanoparticle suspension. The prepared RuO_2/Pt catalysts for electrochemical measurement had nominal Pt loadings of 15, 12, 9, and 5%, which were calculated from the energy-dispersive X-ray (EDX) analysis.

Electrochemical measurement.— All electrochemical experiments were carried out in an Ar_2-protected conventional three-electrode electrochemical cell using an EG&G 273A potentiostat (Princeton Applied Research). The working electrode was a thin layer of Nafion-impregnated catalyst that was cast on a GC electrode surface. The catalyst layer was obtained in the following way. A slurry was first prepared by sonicating 2 mg RuO_2 or RuO_2/Pt catalyst powder in 50 μL of H_2O and 50 μL of Nafion (5 wt %, Aldrich) for 30 min, forming a dark-green suspension solution. Subsequently, 1 μL of catalyst (0.02 mg) was pipetted onto a glassy carbon electrode with the diameter of 4 mm. Before the surface modification, the GC electrode was polished with 0.3 and 0.05 μm alumina slurries, washed with water, and finally subjected to ultrasonic agitation for 1 min in deionized (DI) water. The catalyst layer was then dried at 80°C in an air oven for 1 h. Large surface areas of Pt gauze and Ag/AgCl served as counter electrode and reference electrode, respectively. All potentials in this study are reported with respect to the Ag/AgCl.

Apparatus.— The morphology, structure, and chemical properties of the Pt nanoparticles and RuO_2 nanorods were characterized by transmission electron microscopy (TEM; Philips, Tecnai 20) and high-resolution transmission electron microscopy (HR-TEM; JEOL JEM 2010F) equipped with an EDX spectrometer (Hitachi HF-2000). The operating voltage on the microscope was 200 kV. To obtain TEM images, the powder was dispersed in isopropanol by ultrasonication, and then deposited on a Cu-carbon grid. Powder X-ray diffraction (XRD, Bruker D8 ADVANCE) with Cu Kα (λ = 1.5406 Å) was carried out at a scanning rate of 0.02°/s in 2θ ranging from 20 to 90°.

Results and Discussion

TEM and XRD characterization of Pt nanoparticles and RuO_2 nanorods.— Figure 1 shows the TEM images of the Pt nanoparticles and RuO_2 nanorods. Figure 1a and Fig. 1c reveal monodispersed Pt nanoparticles with a relatively uniform diameter that is centered at 2.5 nm. The corresponding selected-area electron diffraction (SAED) pattern (Fig. 1b) shows five rings corresponding to the {111}, {200}, {220}, {311}, and {331} planes of a face-centered cubic (fcc) crystal structure lattice that indicates the crystalline nature of the Pt nanoparticle. Figure 1d provides typical low-magnification TEM images of the RuO_2 nanorods, which have diameters of 10–15 nm and lengths up to 100 nm. The nanorods are single crystalline as indicated by the SAED pattern given as an inset in Fig. 1e. The inset shows the rods with the long axis directed along the [001]. The HRTEM image (Fig. 1f) clearly indicates that the structure of the RuO_2 nanorod is highly crystalline, with lattice fringes corresponding to the (110) spacing of RuO_2 (a = 4.489 Å, and c = 3.105 Å, rutile structure).

Figure 2 shows the TEM images of (a) as-prepared Pt nanoparticles attached to the RuO_2 nanorod surface (RuO_2/Pt) and (b) the RuO_2/Pt nanocomposite after heating overnight at 400°C in air. The micrograph shows that the Pt nanoparticles have no morphological changes even after thermal treatment at high temperature. TEM data suggest that the bonding of colloidal Pt nanoparticles to the surface of APTES-modified RuO_2 nanorods is relatively strong. The EDX spectrum indicates that the Pt content in the RuO_2/Pt composite is around 12 wt %.

The as-prepared electrocatalyst RuO_2/Pt nanocomposite (Pt: 12 wt %) was also characterized by powder XRD, as shown in Fig. 3. Even though a small-angle technique was used, all reflections can be ascribed to nanocrystalline RuO_2. The absence of individual peaks corresponding to Pt is likely to be due to the low concentration of Pt in the composite material or the very small size of the Pt particles. Similar findings were observed by Villullas and coworkers, in which there was no Pt characteristic peak when the mole ratio of Pt/Ru was lower than 20:80. Thus, it is believed that the relative intensity of Pt is too small to be detected when the concentration is low.[26]

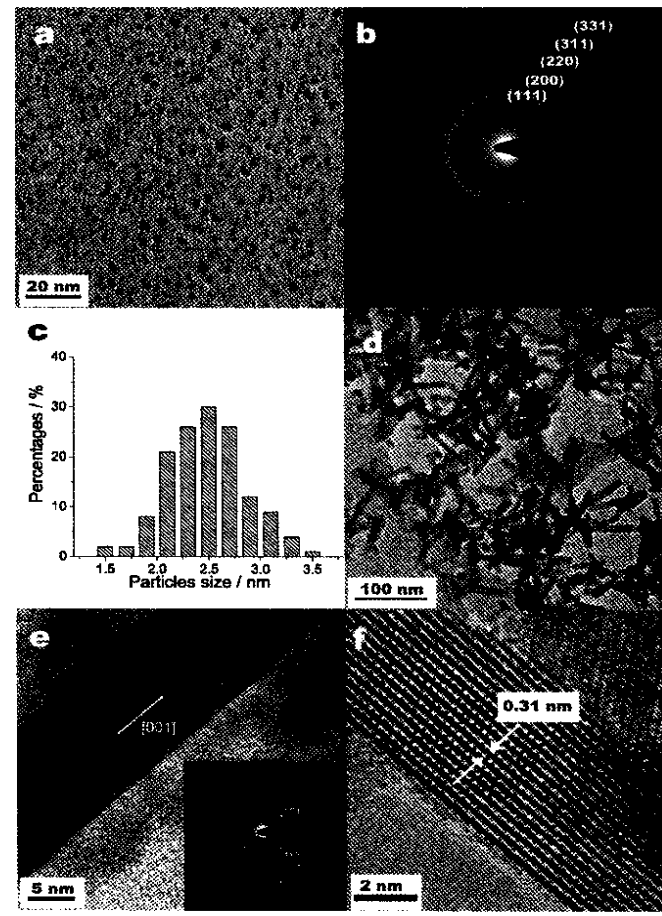

Figure 1. TEM images of the as-prepared Pt nanoparticles: (a) electron diffraction pattern of Pt nanoparticles, indexed to the fcc Pt nanoparticles; (b) the size distribution of Pt nanoparticles; (c) the synthesized RuO_2 nanorods; (d) HR-TEM image of short nanorods (e, f).

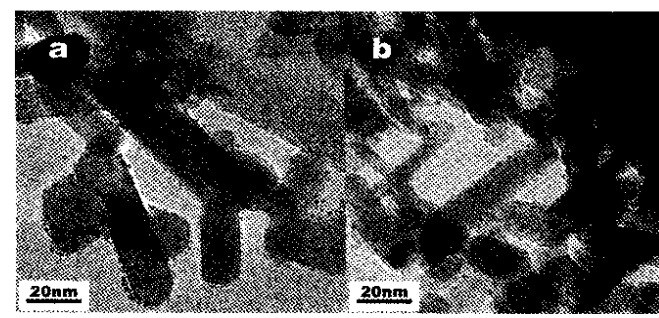

Figure 2. TEM images of the (a) as-prepared Pt nanoparticles attached to the RuO_2 surface-RuO_2/Pt (Pt: 12 wt %); (b) the RuO_2/Pt nanocomposite material after thermal treatment at 400°C for 2 h.

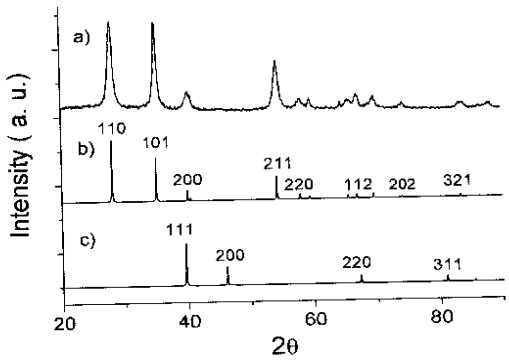

Figure 3. XRD patterns of the RuO_2/Pt nanocomposite (Pt: 12 wt %) (a) with simulated reference patterns of RuO_2 (b) and Pt (c).

Electrochemical performance of RuO_2 and RuO_2/Pt.— Cyclic voltammograms for RuO_2 nanorods, Pt nanoparticles, and RuO_2/Pt nanocomposite in 0.5 M H_2SO_4 are illustrated in Fig. 4. The potential sweep rate is 50 mV/s. The feature of the curve shown in Fig. 4a is very similar to the voltammograms of the single crystal of the RuO_2(110) face.[37] Three regions of hydrogen adsorption, oxide rearrangement, and oxygen adsorption reaction are identified in the whole potential range −0.20–1.20 V. The feature before the anodic-cathodic pair of peaks H_A/H_C (H_2 evolution) can be attributed to H adsorption and desorption. The anodic-cathodic pair of peaks R_A/R_C is in the potential range 0.30–0.70 V due to microstructure defects

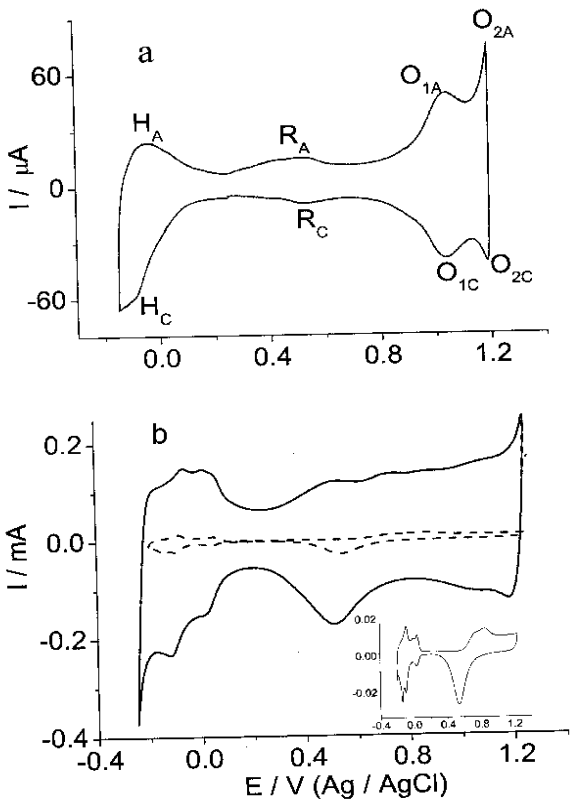

Figure 4. Cyclic voltammograms in 0.5 M H_2SO_4 for RuO_2 (a), RuO_2/Pt (Pt: 12 wt %) (b, solid line) and Pt nanoparticle (b, dotted line) electrodes with a scan rate of 50 mV/s at potential range between −0.20 and 1.20 V. Inset to (b) is a CV of Pt nanoparticles in 0.5 M H_2SO_4.

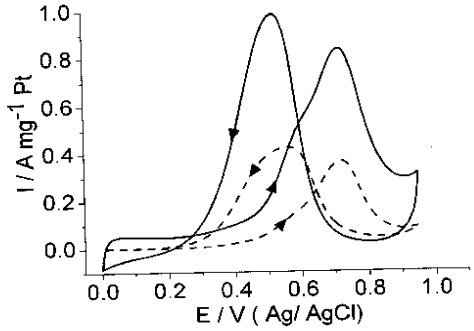

Figure 5. CV for the RuO_2/Pt (solid line, Pt: 12 wt %) and Pt nanoparticle (dotted line) electrodes in 0.5 M H_2SO_4 + 1 M CH_3OH at a scan rate of 50 mV/s.

such as step edges and O vacancies in the surface according to Lister.[37] Two pairs of anodic-cathodic peaks, O_{1A}/O_{1C} and O_{2A}/O_{2C}, are observed in the potential region 0.90–1.20 V. The feature centered near 1.0 V can be attributed to an O adsorption feature. In addition, the O_{2A}/O_{2C} peaks overlap with O_2 evolution on the surfaces. These results are consistent with those observed for the single crystal of RuO_2(110), which suggests that the (110) plane is the predominant crystal plane of the nanorods sidewall. This result is consistent with that determined by the XRD characterization.

The heat-treated RuO_2/Pt catalysts (Pt: 12 wt %; solid line) were characterized by cyclic voltammograms (CV) in 0.5 M H_2SO_4 solution, which are presented in Fig. 4b. The inset of Fig. 4b shows the enlarged CV curve of the as-prepared Pt nanoparticles directly deposited on GC electrode surface in 0.5 M H_2SO_4. The estimated Pt loadings of RuO_2/Pt and the GC electrodes were both about 2.4 μg. The feature of the Pt nanoparticle CV curve is consistent with those of the CV curves for the polycrystalline Pt electrode.[38,39] In the potential region between −0.20 and 0.20 V, hydrogen adsorption and desorption is accompanied with bisulfate desorption and adsorption in the sulfuric acid solution. The peak beyond 0.60 V is due to the oxidation of platinum to form PtO and PtOH during the positive-going potential sweep. The peak at 0.54 V corresponds to the PtO and PtOH reduction during the negative-going potential sweep. The observed hydrogen adsorption and desorption peaks for RuO_2/Pt are similar to those of Pt nanoparticles with the same Pt loading but of a higher intensity and charge, which indicates a higher electrochemical active surface area probably due to the highly dispersed Pt nanoparticles on RuO_2 nanorods. The highly dispersed Pt nanoparticles resulted in fewer nanoparticles overlap and hence provide a higher active surface area than the nanoparticles coated on GC electrode. In contrast, the RuO_2/Pt electrode shows a thick double layer due to the presence of the RuO_2 in the surface layer. Moreover, the onset potential of the surface oxidation for the RuO_2/Pt electrode is 0.30 V, which is significantly lower than that of the Pt nanoparticle electrode (0.60 V). In addition, an increase in current starting at 1.20 V is seen for the RuO_2/Pt electrode, which is attributable to the high activity of RuO_2 toward oxygen evolution.

Electrocatalytic activity for methanol oxidation reaction.— The evaluation of the electrocatalytical activity of the RuO_2/Pt nanocomposites for methanol electrooxidation was performed through cyclic voltammetry in 1 M methanol solution that was contained in 0.5 M H_2SO_4 electrolyte. Figure 5 shows the CV curves in the potential range between 0.0 and 0.95 V for the RuO_2/Pt (solid line) and Pt nanoparticle (dotted line) electrodes. Strong currents were observed at 0.70 V in the forward sweep and 0.45 V in the backward sweep in the CV curves for both electrodes. These two peaks correspond to methanol oxidation.[40] The features of these CV curves are similar except that the RuO_2/Pt electrode produced a higher current density for methanol oxidation. Another significant difference between these

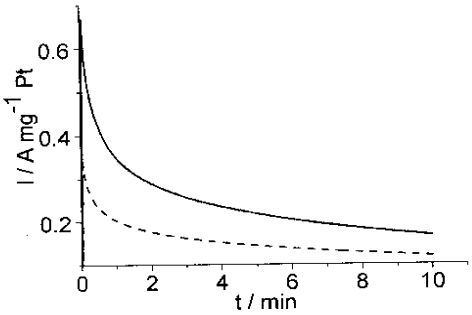

Figure 6. CA curves recorded in 0.5 M H_2SO_4 + 1 M CH_3OH for RuO_2/Pt (solid line) and Pt nanoparticle (dotted line) electrodes at 0.70 V.

two electrodes is the onset potential of methanol oxidation. For the RuO_2/Pt electrode, the onset of methanol oxidation is at approximately 0.20 V, which is 200 mV lower than that for the Pt nanoparticle electrode (0.40 V). The negative shift is similar to that found for Pt-Ru alloy nanoparticles, which indicates that the RuO_2/Pt composite has a positive effect on promoting the oxidation of methanol by lowering its overpotential.[41,42]

Chronoamperometric curve (CA) was applied to further compare the activity of these two electrodes toward methanol oxidation. For this experiment, a potential step from the open circuit potential to 0.20 V was applied immediately after introducing the electrode to the solution. After 10 s at 0.20 V, the potential was then stepped to 0.70 V and the current-time curve was recorded for 3600 s. Figure 6 presents the current-time curves at 0.70 V for the RuO_2/Pt (solid line) and Pt nanoparticle (dotted line) electrodes. The methanol oxidation current at the RuO_2/Pt electrode is higher than that at Pt nanoparticles electrode, although both electrodes display the decay of the current density (which indicates catalyst deactivation).

All of the foregoing CV and CA experimental results show that the RuO_2/Pt electrode has a higher activity for methanol oxidation than that at the Pt nanoparticle electrode. The RuO_2 surface not only disperses Pt more efficiently, but also causes an increase in its electrocatalytical activity in the electro-oxidation of methanol. This increase can be attributed to various factors. It has been reported that RuO_2 has little activity for direct methanol oxidation.[43] Hence, the main role of ruthenium dioxide in the RuO_2/Pt electrode is to promote the electrochemical activity of the Pt catalyst for methanol oxidation, via the so-called bifunctional mechanism. Another factor may be due to the higher dispersion of Pt particles on the surface of RuO_2 nanorods, which can lead to a large number of highly electroactive surface sites that favor the adsorption of OH species at a lower potential. These two effects shift the onset potential of surface oxidation to a negative direction, which induce the onset potential of methanol oxidation shifted from 0.4 to 0.2 V.

Figure 7 shows the CV behavior of different Pt loadings of RuO_2/Pt composition electrodes obtained at a scan rate of 50 mV/s in 0.5 M H_2SO_4 at a potential range of −0.2–0.2 V. The charge for hydrogen adsorption and desorption depends on the electrode composition, which increases as Pt loading increases. This indicates that the real active surface area of the Pt nanoparticles also increased. The voltammetric curves for methanol oxidation on the different Pt loadings of RuO_2/Pt obtained in the potential range between 0.0 and 0.95 V in 0.5 M H_2SO_4 + 1 M CH_3OH solution are shown in Fig. 7b. The features of these CV curves are very similar except that the Pt/MWNTs (Pt: 5 wt %) electrode produced a small current density for methanol oxidation. As shown in Fig. 8, the anodic peak current density increases with the loading of Pt increase. The improved catalytic activity may be due to the increase of the active surface area and the beneficial role of the RuO_2 nanorods. Another significant difference between these samples was the onset potential of methanol oxidation, with RuO_2/Pt (Pt: 15 wt %) catalyst having the

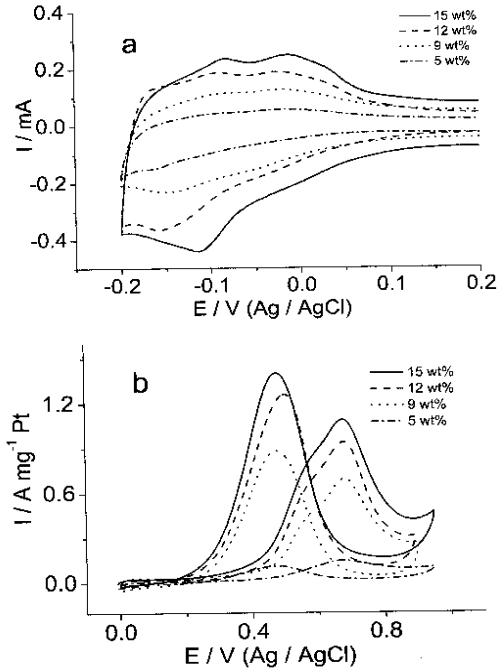

Figure 7. Cyclic voltammograms for different RuO_2/Pt nanocomposites at a scan rate of 50 mV/s in electrolyte of (a) 0.5 M H_2SO_4 and (b) 0.5 M H_2SO_4 + 1 M CH_3OH solution. Pt percent: (– – –) 15 wt %; (- - - -) 12 wt %; (·····) 9 wt %; (- · -) 5 wt %.

lowest value (0.15 V) for methanol oxidation. However, when the Pt loading was lower than 5 wt %, the onset potential of methanol oxidation decreased to 0.40 V and the current density decreased sharply. It is evident that the electrode composition has a significant influence on the behavior toward methanol oxidation. It is reported that anhydrous RuO_2 is rapidly and reversibly oxidized and reduced by electrochemical protonation (Eq. 1)[44]

$$RuO_2 + \delta H^+ + \delta e^- \Leftrightarrow RuO_{2-\delta}(OH)_\delta, \quad 0 \leq \delta \leq 2 \qquad [1]$$

$RuO_{2-\delta}(OH)_\delta$ is a mixed electron-proton conductor and undergoes hydrolysis to give surface Ru-OH bonds, as denoted by Eq. 2

$$Ru^{IV} - O^{2-} + H^+ + e^- \Leftrightarrow Ru^{III} - OH \qquad [2]$$

Similar ruthenium oxide species $RuO_{2-\delta}(OH)_\delta$ formed on the RuO_2 nanorods surface gives the observed enhancement via a similar mechanism proposed by Rolison.[45] The difference in the perfor-

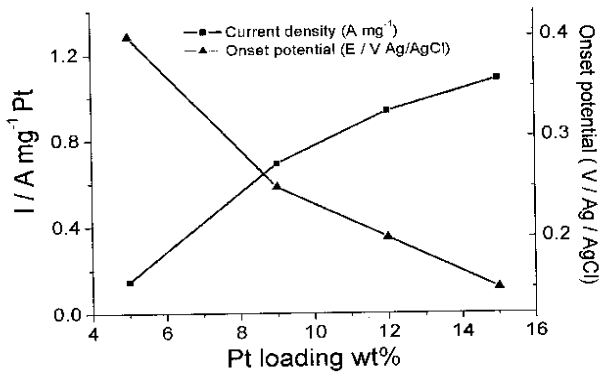

Figure 8. Dependence of current density and onset potential of methanol oxidation on the different Pt loading nanocomposite.

mance of electrodes with different Pt loading could be interpreted by the amount of Pt site where dehydrogenation and oxidation of methanol takes place, that is, the sites where the dissociative adsorption of methanol occurs, and the amount of $RuO_{2-\delta}(OH)_{\delta}$ available for CO to CO_2 conversion. Further study on this aspect is in progress.

The Pt-Ru binary catalysts are known to be very effective anode catalysts for direct methanol fuel cells (DMFC). Massive PtRu alloys and high surface area carbon supported PtRu catalyst have been investigated for their electrocatalytic activities in methanol oxidation.[35,46] Girishkumar and co-workers reported that the PtRu alloy nanoparticles supported on single-walled carbon nanotubes exhibited a ~30% enhancement in the power density of a single stack DMFC, compared to the commercial carbon black support.[46] All the results demonstrated that the electrocatalytic activity of the metal nanoparticles is strongly dependent on the shape, size distribution, loading of the particles, and the support. Because Pt-Ru alloy particles and RuO_2/Pt have entirely different support and Pt loading, it is difficult to cast a good comparison on the electrocatalytic performance of methanol oxidation, although they both exhibit improved catalytic activity.

Conclusions

In this study, the effect of single-crystal structure of RuO_2 nanorods on the electrocatalytic activity of Pt nanoparticles has been investigated by TEM and electrochemical experiments including CV and CA. TEM images of the RuO_2/Pt nanocomposite reveal the homogeneous dispersion of Pt nanoparticles on RuO_2 surface stably attached on RuO_2 surface via a bifunctional ligand of siloxane. The morphology of the RuO_2/Pt nanocomposite showed no significant change even after thermal treatment at 400°C. The electroactive surface area of the RuO_2/Pt nanocomposite is much larger than that of the as-prepared Pt nanoparticles directly deposited on the GC electrode surface with the same Pt loading. The presence of the RuO_2 nanorods greatly increases the electrochemical activity of RuO_2/Pt electrodes toward methanol oxidation, not only increasing the current density but also shifting the onset potential of methanol electro-oxidation to over 200 mV lower than that on the Pt nanoparticle electrode. The results described here also demonstrate the ability of metal oxide nanorods to serve as a type of conductive support for fuel cell applications.

Acknowledgments

We gratefully acknowledge the financial support of the Hong Kong Research Grants Council and the University of Hong Kong. Y.J.G. acknowledges the receipt of a postgraduate studentship, 2003–2006, administered by the University of Hong Kong.

The University of Hong Kong assisted in meeting the publication costs of this article.

References

1. M. Krausa and W. J. Vielstich, *Electroanal. Chem.*, **379**, 307 (1994).
2. R. Viswanathan, G. Hou, R. Liu, S. R. Bare, F. Modica, G. Mickelson, C. U. Segre, N. Leyarovska, and E. S. Smotkin, *J. Phys. Chem. B*, **106**, 3458 (2002).
3. C. Bock, C. Paquet, M. Couillard, G. A. Botton, and B. R. MacDougall, *J. Am. Chem. Soc.*, **126**, 8028 (2004).
4. X. Xue, T. Lu, C. Liu, and W. Xing, *Chem. Commun. (Cambridge)*, **12**, 1601 (2005).
5. F. Liu, J. Y. Lee, and W. Zhou, *Adv. Funct. Mater.*, **15**, 1459 (2005).
6. M. Gotz and H. Wendt, *Electrochim. Acta*, **43**, 363 (1998).
7. A. Oliveira-Neto, I. Perez, W. T. Nappom, E. A. Ticianelli, and E. R. Gonzalez, *J. Braz. Chem. Soc.*, **11**, 39 (2000).
8. M. Umeda, H. Ojima, M. Mohamedi, and I. J. Uchida, *J. Power Sources*, **136**, 10 (2004).
9. M. J. Gonzalez, C. H. Peters, and M. S. Wrighton, *J. Phys. Chem. B*, **105**, 5470 (2001).
10. E. Casado-Rivera, D. J. Volpe, L. Alden, C. Lind, C. Downie, T. Va'zquez-Alvarez, A. C. D. Angelo, F. J. DiSalvo, and H. D. Abruna, *J. Am. Chem. Soc.*, **126**, 4043 (2004).
11. K.-W. Park, J.-H. Choi, and Y.-E. Sung, *J. Phys. Chem. B*, **107**, 5851 (2003).
12. F. Liu, J. Y. Lee, and W. Zhou, *J. Phys. Chem. B*, **108**, 17959 (2004).
13. J. T. Moore, D. Chu, R. Jiang, G. A. Deluge, and C. M. Lukehart, *Chem. Mater.*, **15**, 1119 (2003).
14. J. Huang, H. Yang, Q. Huang, Y. Tang, T. Lu, and D. L. Akinsb, *J. Electrochem. Soc.*, **151**, A1810 (2004).
15. T. Frelink, W. Visscher, and J. A. R. Van Veen, *Langmuir*, **12**, 3702 (1996).
16. S. R. Brankovic, N. S. Marinkovic, J. X. Wang, and R. R. Adžić, *J. Electroanal. Chem.*, **532**, 57 (2002).
17. C. Lu, C. Rice, R. I. Masel, P. L. Babu, P. Waszezuk, H. S. Kim, E. Oldfield, and A. Wieckowski, *J. Phys. Chem. B*, **106**, 9581 (2002).
18. C. L. Campos, C. Roldán, M. Aponte, Y. Ishikawa, and C. R. Cabrera, *J. Electroanal. Chem.*, **581**, 206 (2005).
19. A. L. Santos, D. Profeti, and P. Olivi, *Electrochim. Acta*, **50**, 2615 (2005).
20. A. Chen, D. J. La Russa, and B. Miller, *Langmuir*, **20**, 9695 (2004).
21. S. Trasatti, *Electrochim. Acta*, **29**, 1503 (1984).
22. J. P. Zheng, P. J. Cygan, and T. R. Jow, *J. Electrochem. Soc.*, **142**, 2699 (1995).
23. J. W. Long, R. M. Stroud, K. E. Swider-Lyons, and D. R. Rolison, *J. Phys. Chem. B*, **104**, 9772 (2000).
24. K. E. Swider, P. L. Hagans, J. W. Long, and D. R. Rolison, *Langmuir*, **15**, 774 (1999).
25. H. Hoster, T. Iwasita, H. Baumgartner, and W. Vielstich, *Phys. Chem. Chem. Phys.*, **3**, 337 (2001).
26. H. M. Villullas, F. I. Mattos-Costa, and L. O. S. Bulhões, *J. Phys. Chem. B*, **108**, 12898 (2004).
27. H. B. Suffredini, V. Tricoli, L. A. Avaca, and N. Vatistas, *Electrochem. Commun.*, **6**, 1025 (2004).
28. Z. Chen, X. Qiu, B. Lu, S. Zhang, W. Zhu, and L. Chen, *Electrochem. Commun.*, **7**, 593 (2005).
29. L. X. Yang, R. G. Allen, K. Scott, P. A. Christenson, and S. Roy, *Electrochim. Acta*, **50**, 1217 (2005).
30. H. Over, Y. D. Kim, A. P. Seitsonen, S. Wendt, E. Lundgren, M. Schmid, P. Varga, A. Morgante, and G. Ertl, *Science*, **287**, 1474 (2000).
31. S. Wendt, M. Knapp, and H. Over, *J. Am. Chem. Soc.*, **126**, 1537 (2004).
32. Y. J. Gu and W. T. Wong, *J. Cluster Sci.*, In press.
33. PCT Int. Appl. WO9921934. 47 (1999).
34. D. Caruntau, B. L. Cushing, G. Caruntu, and C. J. O'Connor, *Chem. Mater.*, **17**, 3398 (2005).
35. Z. Liu, X. Y. Ling, X. Su, and J. Y. Lee, *J. Phys. Chem. B*, **108**, 8234 (2004).
36. C. Bock, C. Paquet, M. Couillard, G. A. Botton, and B. R. MacDougall, *J. Am. Chem. Soc.*, **126**, 8028 (2004).
37. T. E. Lister, Y. Chu, W. Cullen, H. You, R. M. Yonco, J. F. Mitchell, and Z. Nagy, *J. Electroanal. Chem.*, **524**, 201 (2002).
38. Z. Liu, J. Y. Lee, W. Chen, M. Han, and L. M. Gan, *Langmuir*, **20**, 181 (2004).
39. U. A. Paulus, A. Wokaun, G. G. Scherer, T. J. Schmidt, V. Stamenkovic, N. M. Markovic, and P. N. Ross, *Electrochim. Acta*, **47**, 3787 (2002).
40. P. J. Kulesza, M. Matczak, A. Wolkiewicz, B. Grzybowska, M. Galkowske, M. A. Malik, and A. Wieckowski, *Electrochim. Acta*, **44**, 2131 (1999).
41. M. J. González, C. T. Hable, and M. S. Wrighton, *J. Phys. Chem. B*, **102**, 9881 (1998).
42. M. J. González, C. H. Peter, and M. S. Wrighton, *J. Phys. Chem. B*, **105**, 5470 (2001).
43. B. J. Kennedy and A. W. Smith, *J. Electroanal. Chem. Interfacial Electrochem.*, **293**, 103 (1990).
44. J. P. Zeng, Q. X. Jia, X. D. Wu, and J. R. Jow, *J. Electrochem. Soc.*, **143**, 1068 (1996).
45. J. W. Ling, R. M. Stoud, K. E. Swider-Lyons, and D. R. Rolison, *J. Phys. Chem. B*, **104**, 9772 (2000).
46. G. Girishkumar, T. D. Hall, K. Vindgopal, and P. V. Kamat, *J. Phys. Chem. B*, **110**, 107 (2006).